ISSN 0015-4628, Fluid Dynamics, 2022, Vol. 57, No. 3, pp. 371–386. © Pleiades Publishing, Ltd., 2022.

# Experimental Investigation of the Effect of a Semi-Circular Spiral Protrusion on the Turbulent Flow Past a Cylinder

**F. Koca[a],* and A. Ozturk[a],****

[a]*Sivas Cumhuriyet University, Sivas, Turkey*

**e-mail: ferhatkoca@cumhuriyet.edu.tr*

***e-mail: aozturk@cumhuriyet.edu.tr*

Received July 1, 2021; revised September 29, 2021; accepted October 5, 2021

**Abstract**—The effect of semi-circular spirals on a circular cylinder surface to flow structure was experimentally investigated by the particle imaging velocity measurement (PIV) method. Based on the PIV channel, the main body cylinder length was determined as 440 mm. The single coil ($p$ = 440 mm), double coils ($p$ = 220 mm) and quadruple coils ($p$ = 110 mm) structures were formed by changing the number of steps ($p$) of the semi-circles on the cylinder surface. The flow structure has been examined in six different planes according to the position of the helix. The Reynolds number studied is 10000, depending on the average fluid velocity in the PIV channel and the main body cylinder diameter ($D$). The time-averaged streamline $\langle\psi\rangle$, the turbulent kinetic energy $\langle$TKE$\rangle$, the root mean square (RMS) of streamwise velocity $U_{\text{rms}}$, the root mean square (RMS) of cross-stream velocity $V_{\text{rms}}$ and the Reynolds shear stress $\langle u'v'\rangle$ were obtained. The Strouhal numbers were calculated using the Karman vortex frequencies. It is concluded that the spirals on the cylinder reduce the vibrations caused by the vortex.

**Keywords:** PIV, semi-circular cylinder, flow control, helical wing

**DOI:** 10.1134/S0015462822030089

In engineering applications, special flow areas on objects such as high-rise buildings, bridges, cooling towers, chimneys, tubes in heat exchangers are frequently encountered. Because of the shape of these objects, there is a considerably large area behind them where the flow circulates. This area is called the wake region and there is a pressure drop in these regions. Furthermore, the phenomenon of vortex shedding created by flow separation from the body creates an unstable periodic force which causes the large body vibration and may lead to structural distortion. Therefore, the knowledge of the flow field around these structures is of great importance in many applications such as civil engineering, mechanical engineering, and technical problems related to energy conversion and structural design. Understanding of the flow structure is also important to limit the oscillation amplitude as well as prevent resonance. The resonance event of the Tacoma Narrows Bridge in 1940, when the frequency of vortex shedding is higher than the natural frequency of the structure, is the subject of almost all physics books. It is important to know and control the flow structures so that such events do not occur. Flow control research is based on the discovery of the boundary layer by Prandtl [1] in the early 20th century. Two methods can be applied to control the flow around a blunt body. One of them is the method called the passive control, in which the surface geometry is changed by placing protrusion lines or cavities on the surface. The other is the active control methods in which the external energy is supplied to the flow area with applications such as blowing, suction, synthetic jets and plasma actuators under certain conditions, the electric discharge etc. In flows around such bodies, the behavior of the flow changes as the Reynolds number increases. The basic fluid dynamics problems of objects such as circular and rectangular cylinders have been extensively studied both numerically and experimentally at various Reynolds numbers [2–10]. In [11] the effect of spiral geometries on a cylinder on vortex induced vibration (VIV) was investigated. The spiral structures placed in a water channel with different pitches ($p$ = 5, 10, 15d) and heights ($h$ = 0.1, 0.2, 0.25d) with Reynolds numbers varying between 1000 and 10000 were examined. It was shown that $h$ = 0.2d and $h$ = 0.25d helix structures almost completely suppress VIV. In [12] the flow characteristics at 6250 Reynolds number with the plate passive control method placed on the cylinder using the PIV method were studied. It was found that with increase in the length of the plate, its effect on suppression of vortex shedding increased. In [13] the experimental study was conducted to examine the VIV of fixed circular cylinders with three helical grooves. It was emphasized that the spiral grooves were effective in suppressing the vor-

**Fig. 1.** General view of the water channel.

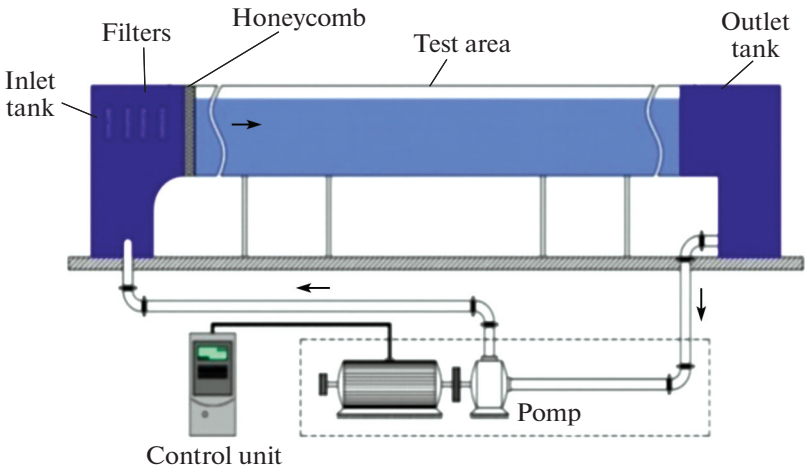


**Fig. 2.** Schematic view of the experimental setup.

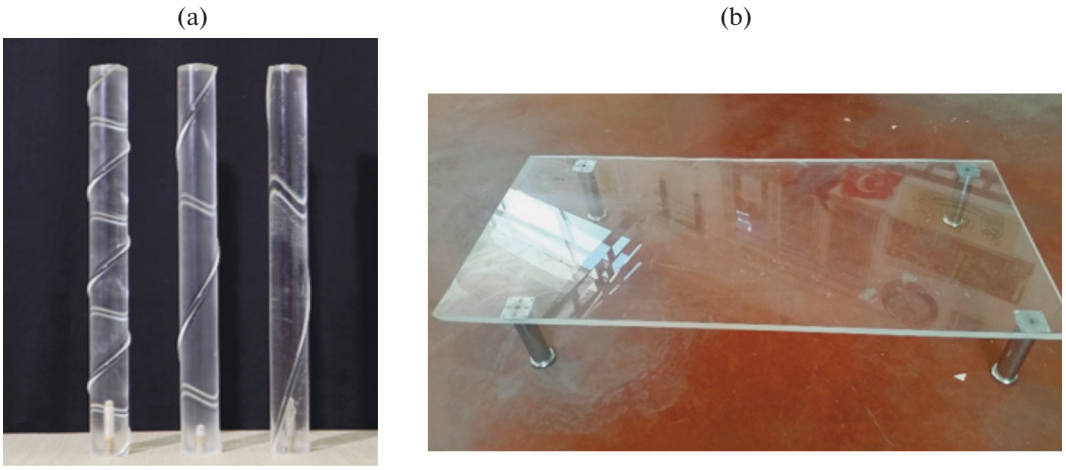


**Fig. 3.** Test materials (a) models (b) platform.

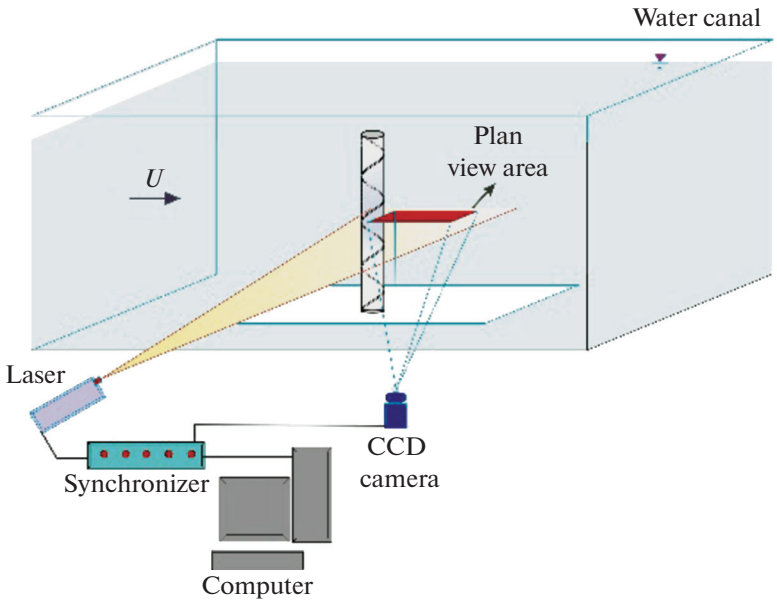


**Fig. 4.** Schematic of test equipment and digital PIV devices.

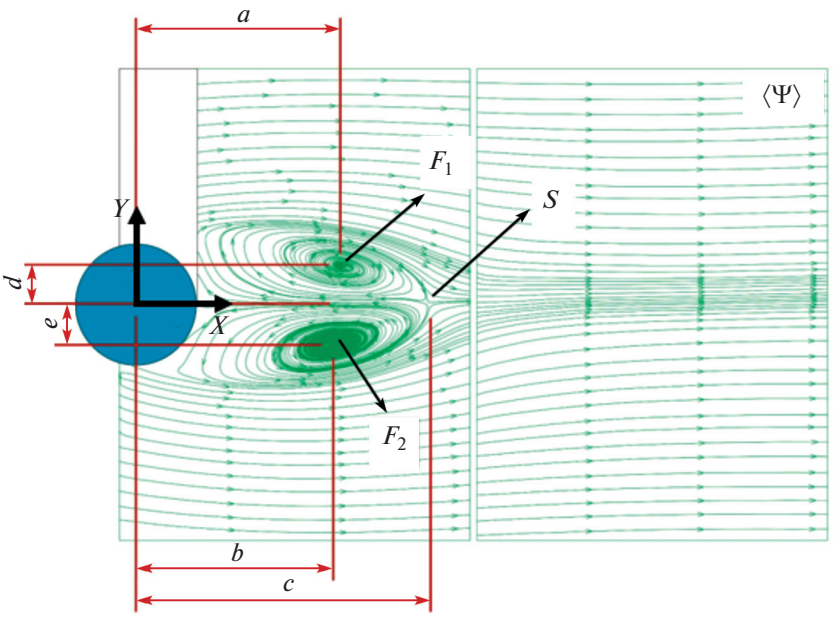


**Fig. 5.** Streamlines and important points.

tex-induced cross flow vibration amplitudes and that the peak amplitude was reduced by 64%. In [14], which is also an experimental study, the effects of a single straight and three spiral wires wrapped on a circular cylinder surface on critical flow in homogeneous cross flow were investigated. The experiments were carried out at Re = 10000 (depending on the cylinder diameter) using a cylinder with the outer diameter $D = 50.8$ mm. In the study, it was stated that the spirals have a significant effect on the vortex-induced vibrations. In [15] the study on the confined flow over a circular cylinder with a splitter plate was investigated experimentally. The 30 mm diameter plexiglass cylinder into the channel at a 0.3 blockage rate was placed. The separator plate length $L/D$ (here, $L$ is the plate length and $D$ is the cylinder diameter) between

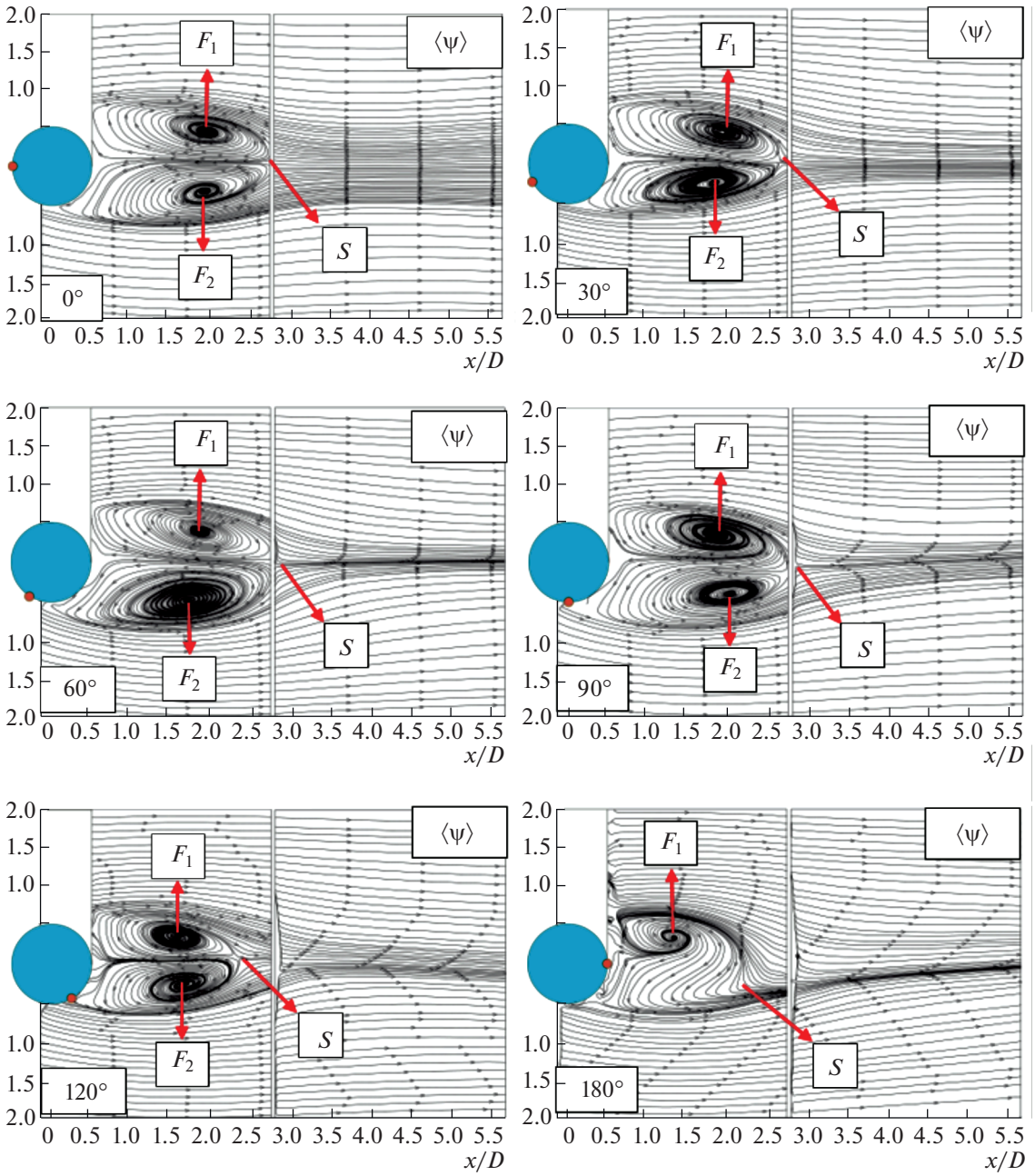


**Fig. 6.** Streamlines of single coil for the angular positions θ = 0°, 30°, 60°, 90°, 120°, 180° relative to the cylinder stagnation point.

0 and 1.5 and the Re numbers between 2400 and 3000 were varied. It was noted that for short plate lengths the flow pattern was modified significantly compared to the flat cylinder, the vortex spill frequency was reduced, and secondary vortices occur for long plates.

The aim of the study is to examine the effect of the spiral structures designed on the cylinder placed in the channel using the PIV method on the flow. The PIV data were processed in dif locations along the cylinder and made for the placement of the spiral and for a certain Re number, the flow and turbulence distributions were given, the vortex shedding that are effective in vibration control were examined, and important flow parameters were calculated.

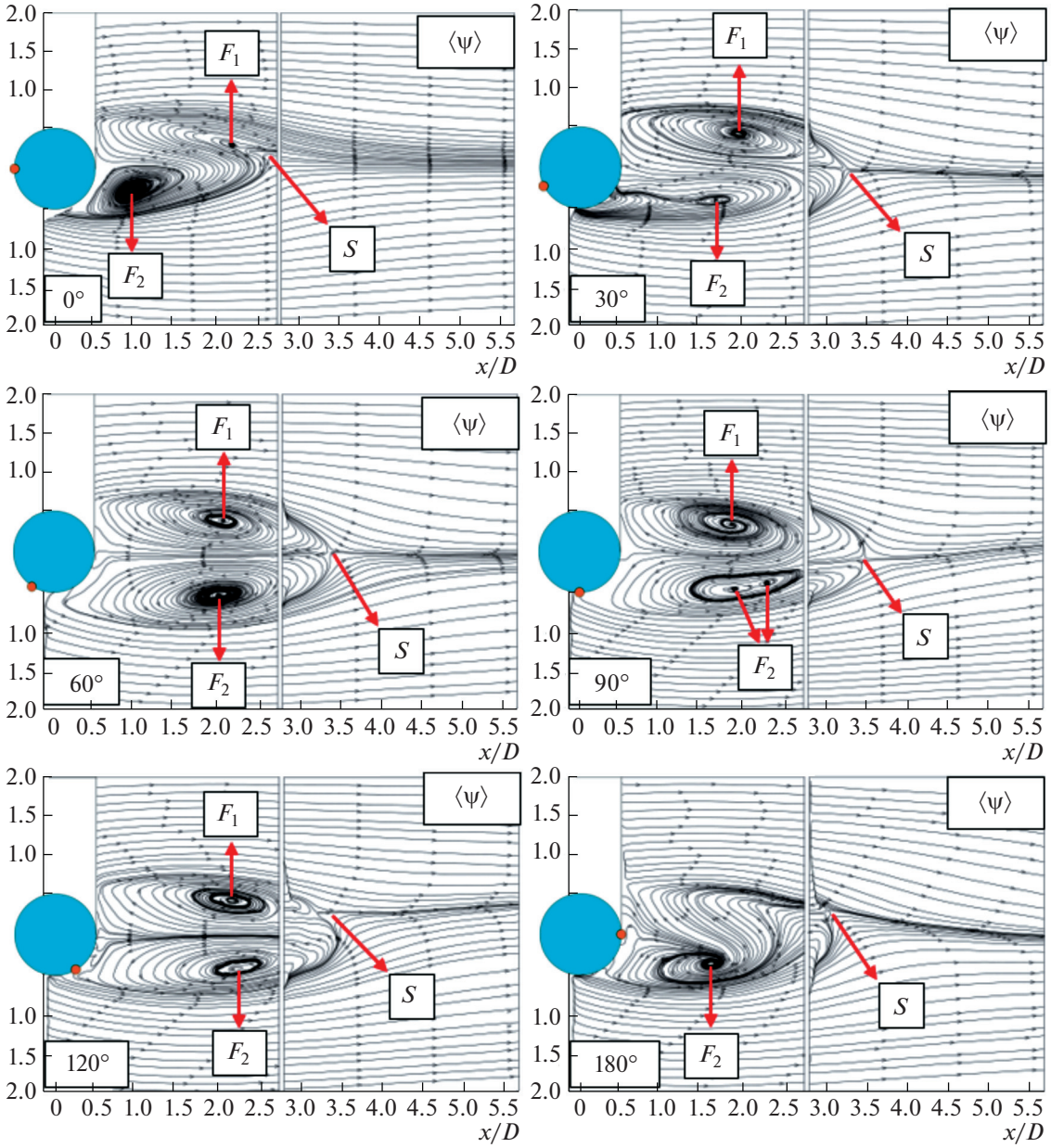


**Fig. 7.** Streamlines of double coils for the angular positions θ = 0°, 30°, 60°, 90°, 120°, 180° relative to the cylinder stagnation point.

## 1. EXPERIMENTAL SET-UP

In this study, the flow structure around three finite-cylinders with spirals of different pitches attached to their surfaces was experimentally investigated in a closed circuit open surface water channel using the particle imaging velocity (PIV). Figure 1 shows the water channel in Osmaniye Korkut Ata University, Faculty of Engineering, Department of Energy Systems Engineering, Fluid Dynamics Laboratory where the experiments were conducted. Figure 1 location (after this paragraph).

The basic components of the water channel are shown in Fig. 2. Accordingly, the system consists of a control panel that controls the motors connected to the water channel, inlet and outlet collection chambers and a test room.

The experiments were carried out at Re = 10 000 based on free flow velocity and finite cylinder diameter. The effects of the cylinder surface on the flow area were discussed by processing the obtained data in computer environment.

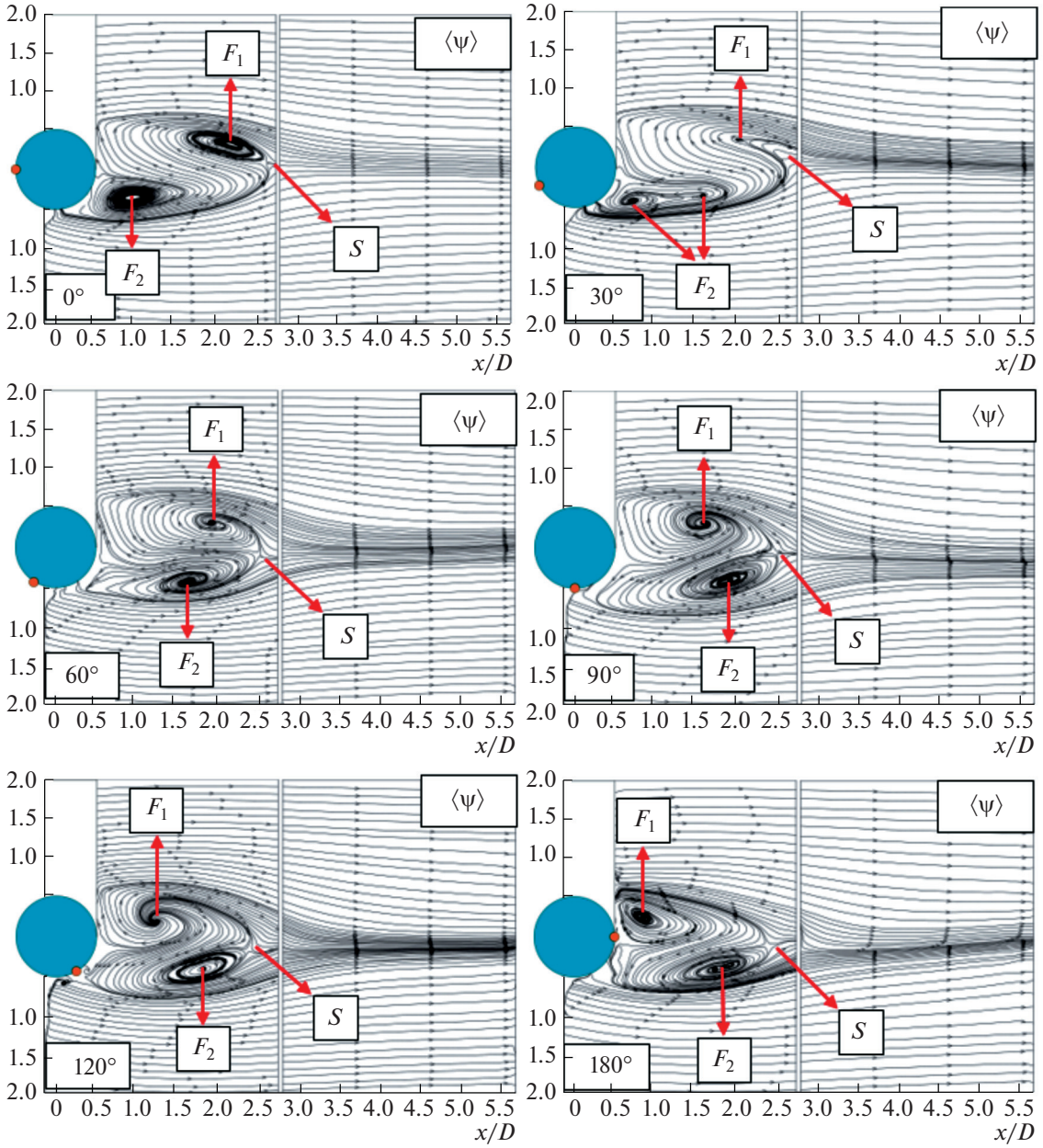


**Fig. 8.** Streamlines of quadruple coils for the angular positions θ = 0°, 30°, 60°, 90°, 120°, 180° relative to the cylinder stagnation point.

## 2. MODELS

The cylinder models used in the experiments are shown in Fig. 3. A total of 4 experimental models, 3 models consisting of single, double and quadruple coils, and a bare cylinder were used. The single coil ($p$ = 440 mm), double coils ($p$ = 220 mm) and quadruple coils ($p$ = 110 mm) structures were formed by changing the step number ($p$) of the semi-circles on the cylinder surface. The models were made of plexiglass material. The test cylinders were obtained by processing 50 mm diameter plexiglass tubes using a high precision computer numerical control (CNC) milling machine. The $L/D$ (length/diameter) ratio of the cylinders and the $D/d$ (cylinder diameter/winding diameter) ratio of the half-cylinder spiral windings on the cylinder surface were processed to be 10. The length of the main cylinder is limited to 440 mm to prevent deterioration in the structure of the material during processing. The experiments were carried out on a platform placed in the water channel. The platform is shown in Fig. 3. The length of the platform is equal to 1500 mm, its width is equal to 700 mm, the height of the platform from the base of the channel

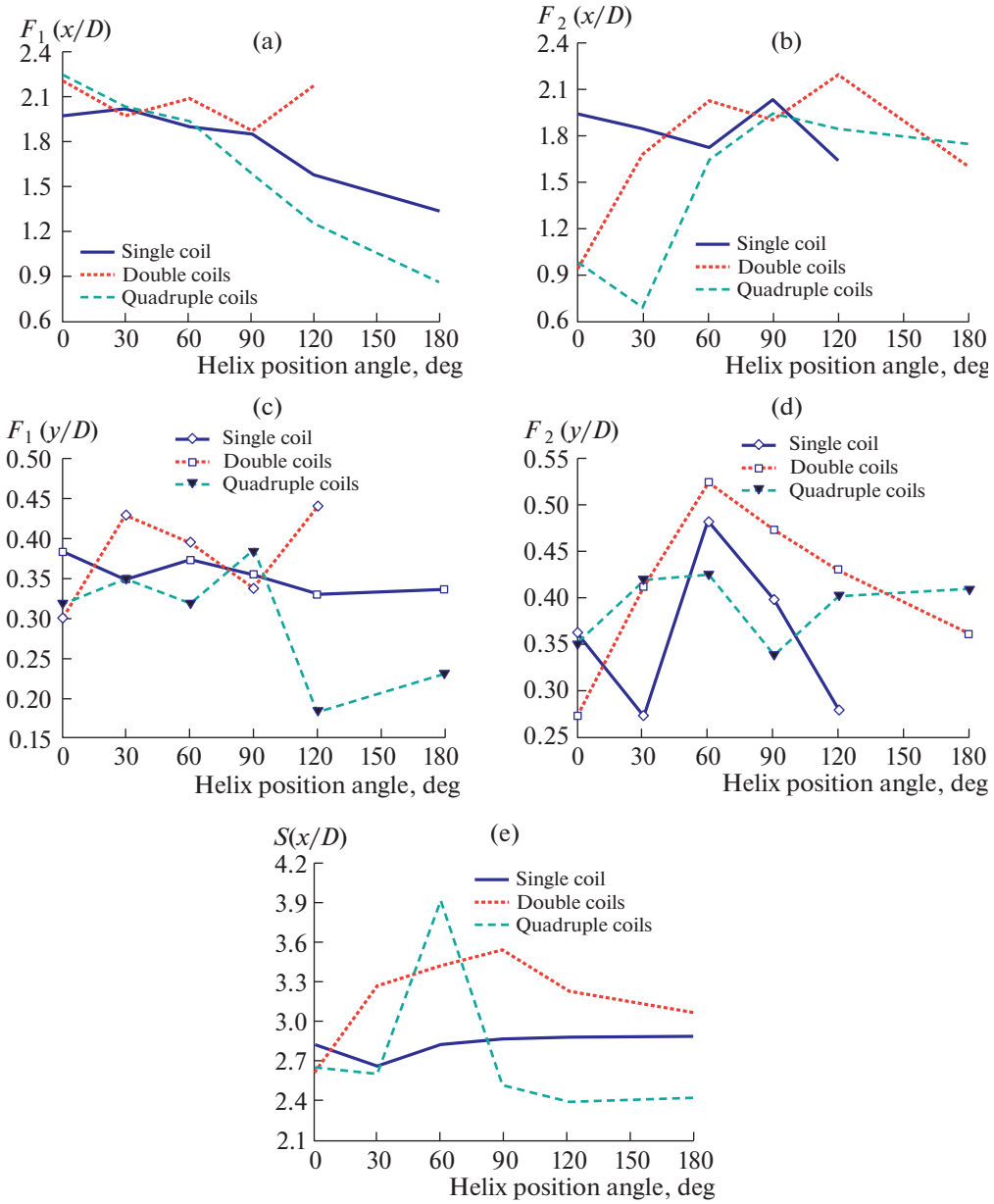


**Fig. 9.** Helix angle position–dimensionless distance of the critical point graphs: (a) $F_1\,(x/D)$—helix position, (b) $F_2\,(x/D)$—helix position, (c) $F_1\,(y/D)$—helix position, (d) $F_2\,(y/D)$—helix position, (e) $S\,(x/D)$—helix position.

is equal to 220 mm, and the distance between the platform and the water surface is set equal to 600 mm. The experiments were conducted by mounting test cylinders on this platform. The Reynolds number is calculated as 10000 depending on the main cylinder diameter and the channel free flow velocity. The experiments were carried out at the angular position of the windings $\theta = 0°$, 30°, 60°, 90°, 120°, and 180° relative to the cylinder stagnation point to investigate the effect of the angular position. During the experiments, 1000 snapshots were recorded for each angular position. The velocity vectors were calculated by processing the obtained images. Flow characteristics were determined by using these data.

The cylinders was not revolved of getting data for different angular positions of the spiral. Instead of that the measurement plane was shifted along the cylinder axis. The getting data of zero helix angle for all models was made from the $z/D = 5$ point, which is the middle point of the cylinder. For every 30° increment, 36.67 mm for single coil, 18.33 mm for double coils, 9.16 mm for quadruple coils, laser positions was moved along $Z$ axis without rotating the cylinder.

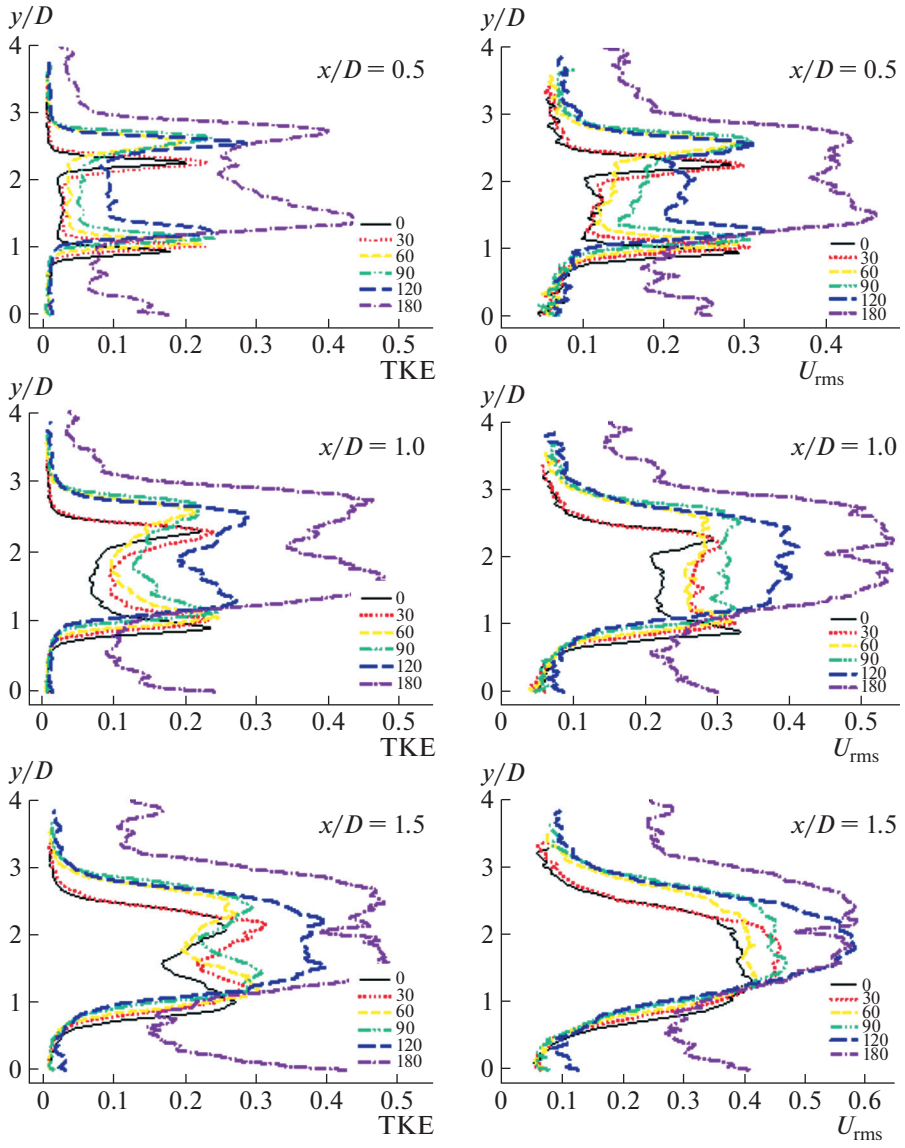


**Fig. 10.** Turbulent kinetic energy (TKE) and root mean square velocity $U_{rms}$ distributions at various fluid locations within a single coil wake region.

The scheme of the PIV system used in this study is shown in Fig. 4. During image acquisition, the flow field was illuminated by a double-pulsed Nd : Yag (neodymium-doped yttrium aluminum garnet) laser unit in a plane perpendicular to the flow. For all measurements, the time interval between two laser pulses was set to be equal to 83 ms. The water flow was seeded with 10 μm diameter particles, added with a minimum of 50 particles on each image screen. The motion of these particles was recorded using a CCD camera. The recorded images were processed using Dantec Flow Manager software.

In this experimental study, hollow glass spheres (HGS-10) of 10 μm diameter were added to the water used as working fluid. The properties of the HGS-10 particles used are given in Table 1.

## 3. EXPERIMENTAL RESULTS

The time-averaged flow structure around the bare cylinder has symmetry about the $X$ axis [17, 18]. Time-averaged streamline ($\psi$) patterns reveal that a pair of focus points ($F_1$ and $F_2$) with opposite directions of circulation is formed in the wake region of a circular cylinder. This circulation zone is bounded by

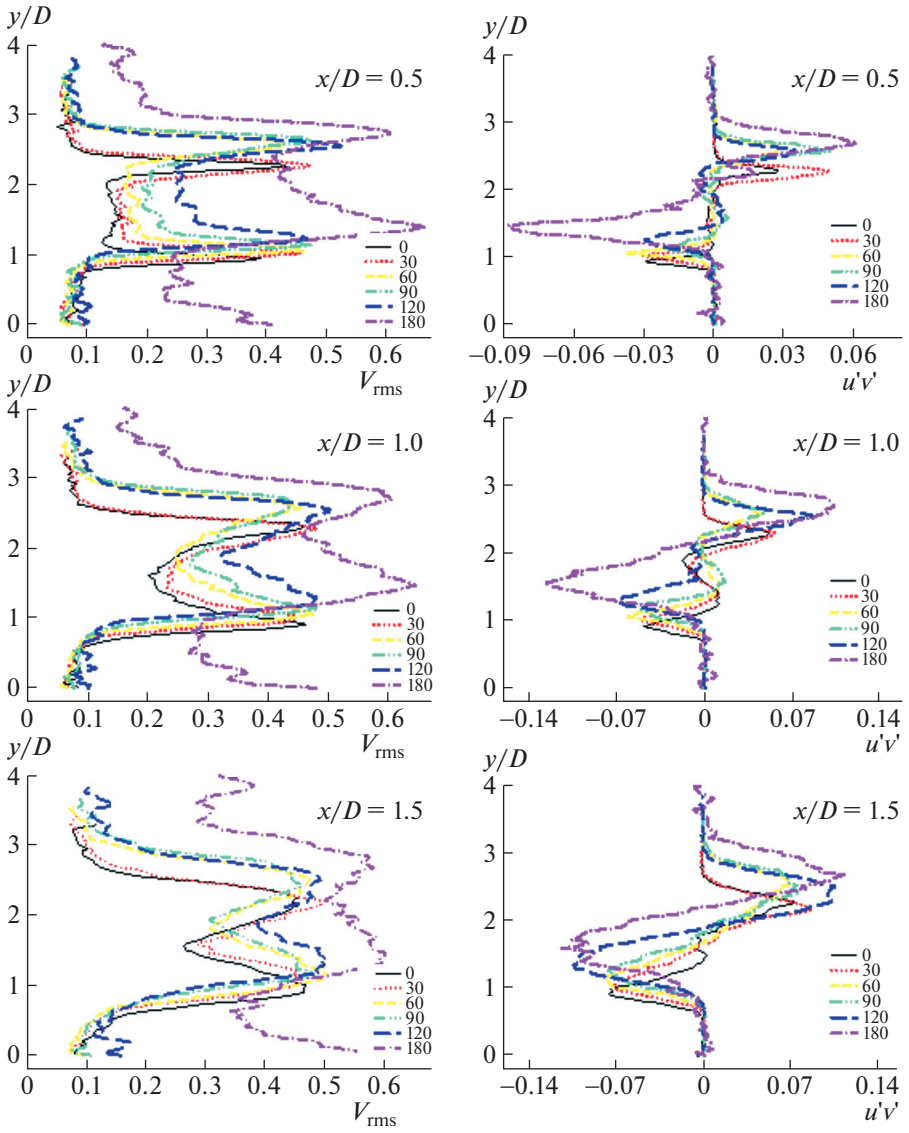


**Fig. 11.** Root mean square $V_{rms}$ and Reynolds stress correlation distributions at various fluid locations within the single coil wake region.

the free flow leaving a saddle point ($S$) downstream of the flow field. The presentation of the obtained findings in the study is compatible with the literature [19–21].

Figure 5 shows the wake region streamlines and important points in this region. The positions (a, b, c, d, e) of the important points ($F_1$, $F_2$, and $S$) in these streamlines obtained as a result of processing 1000 images taken from the PIV, according to the $X$ and $Y$ axes have been extracted. As the $X$–$Y$ axes, the origin point

**Table 1.** HGS-10 particle properties [16]

| | HGS (hollow glass spheres) |
|---|---|
| Average particle size, μm | 10 |
| Particle shape/material | Spherical/borosilicate glass |
| Density, g/cm$^3$ | 1.1 |
| Melting point, °C | 740 |
| Refractive index | 1.52 |

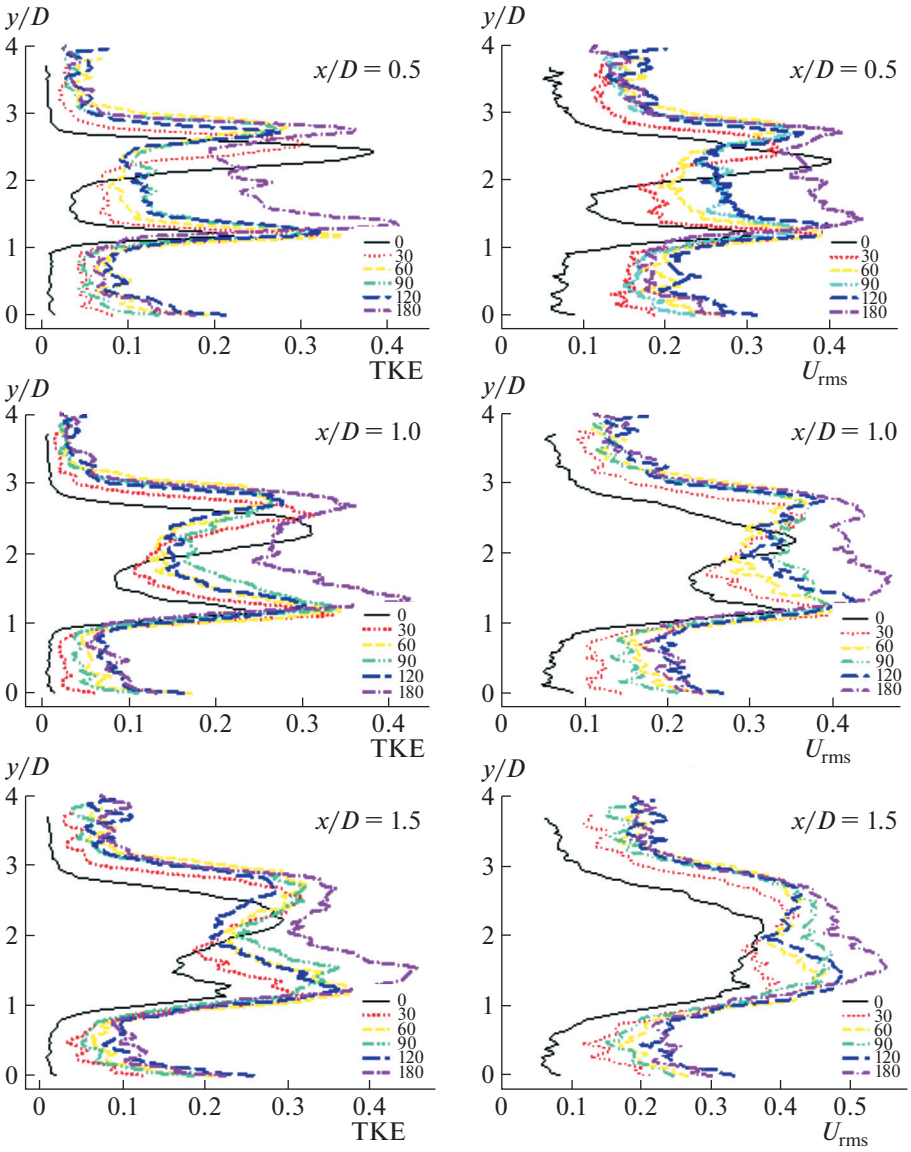


**Fig. 12.** Turbulent kinetic energy TKE and root mean square velocity $U_{rms}$ distributions at various fluid locations within the double coils wake region.

($X = 0$, $Y = 0$) was determined as the midpoint of the cylinder. The time-averaged streamline is first derived for a bare cylinder made without a spiral structure, in Fig. 5, and then for cylinders manufactured in different spiral steps. The critical points ($F_1$, $F_2$, and $S$) were obtained as dimensionless $x/D$ and $y/D$ (depends on main body cylinder diameter $D$) for angular positions θ = 0°, 30°, 60°, 90°, 120°, and 180° relative to the free flow axis.

Figure 9 shows the graphs of values of the dimensionless critical point obtained from the streamlines with variation in the helix angle. Since it is the angle value that disturbs the flow structure the most, it is clearly seen from the graphs that the helix 90° angle is the critical angle. The double coils cylinder shows a more horizontal transition impression with variation in the helix angle compared to the other cylinders. It also has greater values. Therefore, it is determined that the wake region is spread over a wider area.

For all θ (0°, 30°, 60°, 90°, 120°, and 180°) the states at various locations; the turbulence kinetic energy distribution, the root mean square of the streamwise velocity component $U_{rms}$ and the root mean square of the cross-stream velocity component $V_{rms}$ and the Reynolds shear stress correlations $u'v'$ are shown in

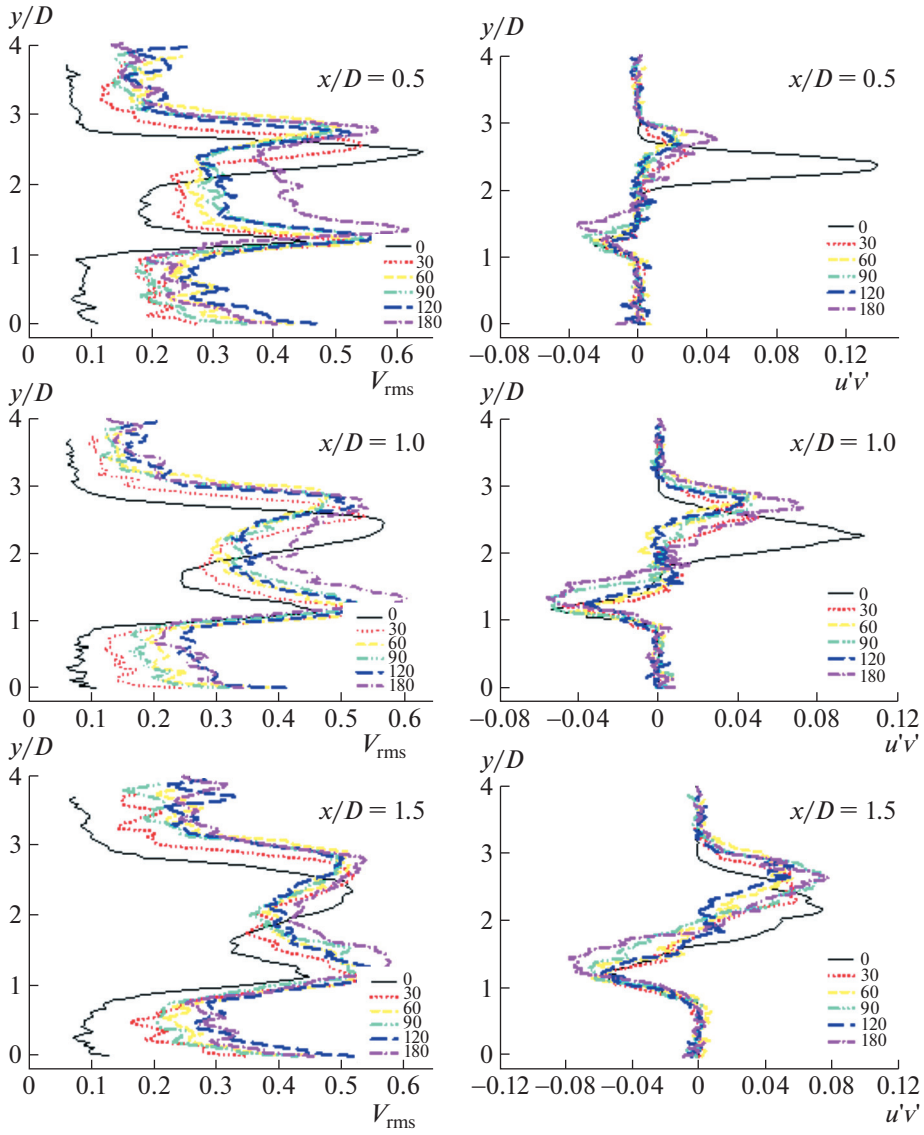


**Fig. 13.** Root mean square velocity $V_{rms}$ and Reynolds stress correlation distributions at various fluid locations within the double coils wake region.

this section. In this study only the 2D flowfield is considered due to the nature the PIV setup used here, and so the full three-dimensional definition of TKE, $k$, was simplified in the forn of expression (3.1):

$$k = \frac{1}{2}[\overline{u'u'} + \overline{v'v'}]. \tag{3.1}$$

The obtained TKE values were nondimendionalized by means of the 0.41 free flow velocity used for Re = 10000. Also graphics were obtained at $x/D$ dimensionless distances. The position $x/D = 0.5$ was randomly chosen to reveal the development of turbulence statistics immediately behind the cylinder. The dimensionless position of $x/D = 1$ is determined to the vertical focal points, and the dimensionless position of $x/D = 1.5$ is determined approximately to the position of the saddle point. The magnitudes of the $U_{rms}$ and TKE initially increase with the distance from both sides of the cylinder and then decrease by obtaining a local maximum value in the shear layer. However, at $x/D = 0.5$ the sizes appear to decrease significantly the local maximum. Moreover, the graphs of the TKE have a relatively weak secondary local peak around the boundary of circulation line of the corresponding streamline. The distance between the local peaks of the TKE on both sides decreases as the streamline gets longer with downstream distance. On both sides the maximum points of the graphs of $U_{rms}$, $V_{rms}$ and TKE approach each other with increase

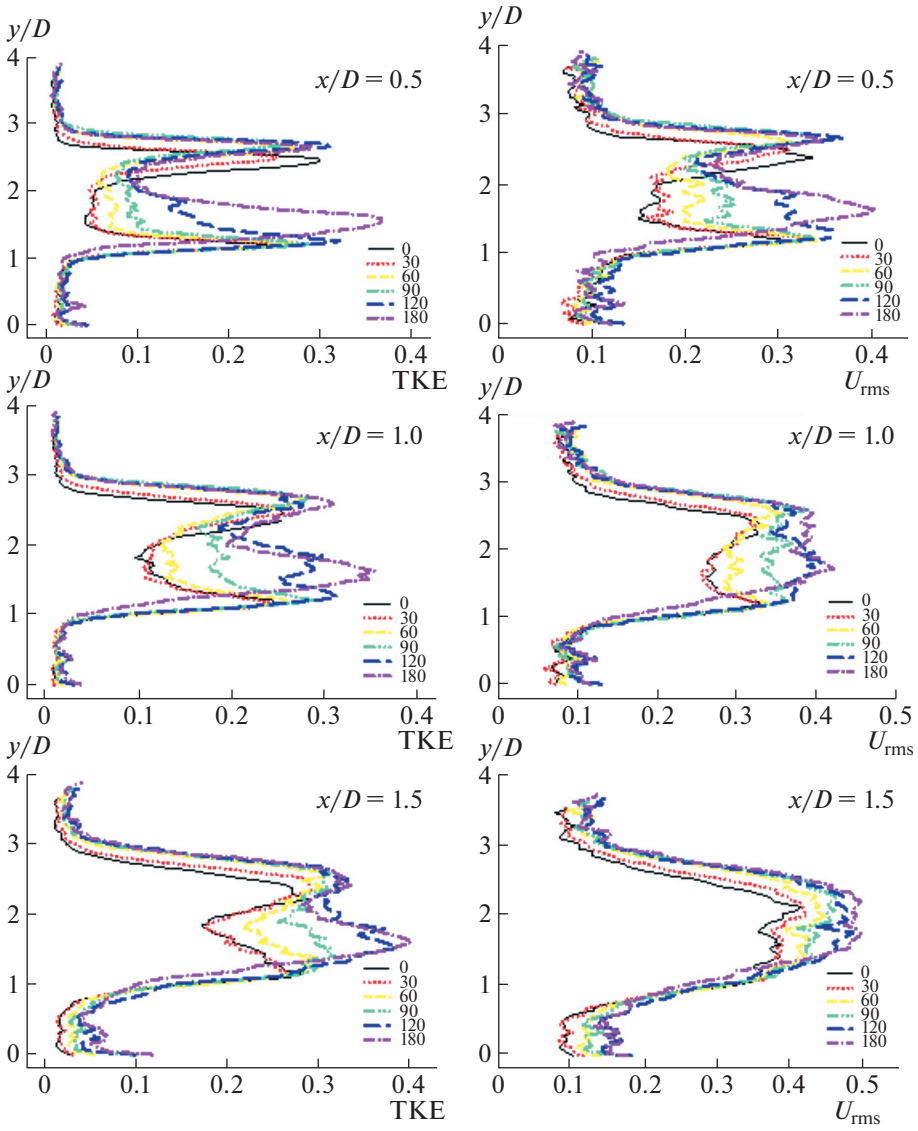


**Fig. 14.** Turbulent kinetic energy TKE and root mean square velocity $U_{rms}$ distributions at various fluid locations within the quadruple coils wake region.

in the distance in the direction of flow. When the graphs of the Reynolds stress correlation are examined, it is seen that the dimensionless distance $x/D$ increases, it shows the sinusoidal distribution. Two local peaks occurring just above and below the streamline circulation line near the cylinder transform from vertical to more inclined. All obtained results are shown in Figs. 10–15.

In Fig. 16 we have shown the power spectrum of the velocity investigated at the points of the flow field in order to determine the Karman vortex shedding frequency $f$ and the irregularities in the shear layer. First, two points on either side of the cylinder, designated $A$ and $B$, are identified to determine the dominant frequencies. Point $A$ was determined at a dimensionless distance equal to 3 from the $x$ axis and 0.5 from the $y$ axis depending on the cylinder diameter, and the point $B$ was determined to be $x/D = 3$ and $y/D = 0.5$ symmetrically to the cylinder center line with respect to point $A$.

In Table 2 we have given the frequency, the period and the Strouhal numbers obtained at the $A$ and $B$ points for the bare cylinder and three model cylinders with spiral structure. The table uses 1 s for the single coil model, 2 s for the double-coils model, and 4 s for the quadruple-coils model, and the plane degrees are indicated next to them. Period values ($1/f_A$ and $1/f_B$) and Strouhal ($fD/U$) number values for $A$ and $B$ points were obtained by mathematical transformations. When the table is analyzed, the bare cylinder with the $f = 1.096$ dominant frequency corresponding to the St = 0.21 Strouhal number is compatible with the

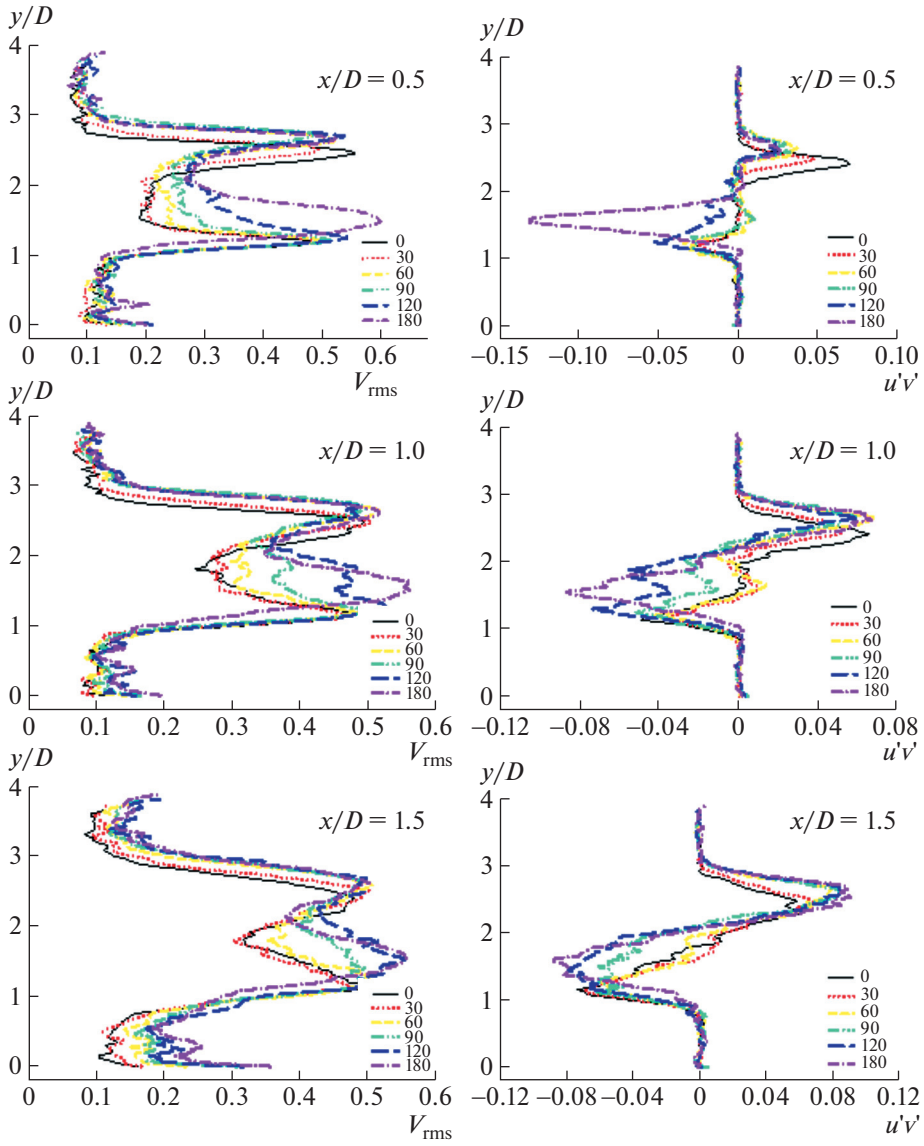


**Fig. 15.** Root mean square $V_{rms}$ and Reynolds stress correlation distributions at various fluid locations within the quadruple coils wake region.

results [22]. When Table 2 is examined, the minimum frequency of 0.878 at point *A* is obtained for the double coil structure where the helix position is equal to 120° (2s120). Figure 17 shows variation in St as a function of the helix angle.

## SUMMARY

In this study, the flow structure around a circular cylinder was investigated using the particle imaging velocity measurement (PIV) technique, using the angular position of the spiral on the cylinder as a function of the stagnation point of the cylinder. A total of 4 experimental models, 3 models consisting of single, double and quadruple coil numbers and bare cylinder, were used. The Reynolds number based on cylinder diameter has been calculated as 10000. The experiments were carried out at the angular positionsInlt of the windings $\theta = 0°$, 30°, 60°, 90°, 120°, and 180° relative to the cylinder stagnation point to investigate the effect of angular position.

The experimental results on the straight cylinder (without helix) are consistent with the available literature. It has been observed that the flow structure has a profound effect on turbulence statistics and vortex

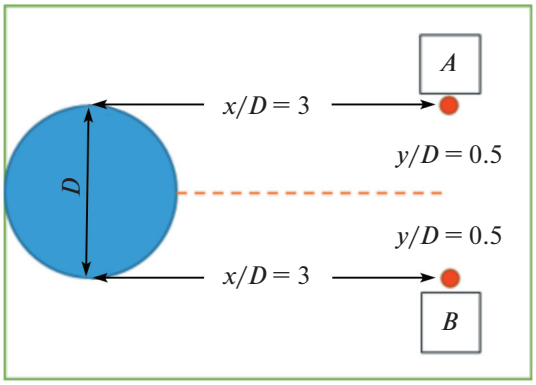


**Fig. 16.** FFT analysis spectrum points.

shedding frequency. The critical points $F_1$, $F_2$, and $S$ of the flow on the bare cylinder are always located further downstream of the cylinder than the cylinders with helices. Asymmetry is observed in the wake region of the flow structure and this affects the distribution of turbulent statistical lines. The Strouhal number (St) varies as a function of the θ and the St number takes its maximum value at 90°. Therefore, it is thought that the single semicircular cylinder formed by winding on the circular structure can be used to reduce the flow-structure interaction and flow control. It is concluded that the spiral structures on the cylinder significantly affect the downstream region, decrease the velocity fluctuation magnitudes, thus

**Table 2.** Frequency, period and Strouhal number

| | $F_A$ | $F_B$ | $T_A$ | $T_B$ | $T_A$, s | $T_B$, s | $St_A = fD/U$ | $St_B = fD/U$ |
|---|---|---|---|---|---|---|---|---|
| Straight | 1.096 | 1.096 | 0.912 | 0.912 | 10.99 | 10.99 | 0.212 | 0.212 |
| 1s0 | 1.023 | 1.032 | 0.977 | 0.968 | 11.78 | 11.67 | 0.197 | 0.199 |
| 1s30 | 1.041 | 1.031 | 0.960 | 0.969 | 11.57 | 11.69 | 0.201 | 0.199 |
| 1s60 | 1.062 | 1.069 | 0.941 | 0.935 | 11.34 | 11.27 | 0.205 | 0.206 |
| 1s90 | 0.947 | 0.974 | 1.055 | 1.026 | 12.72 | 12.37 | 0.183 | 0.188 |
| 1s120 | 0.954 | 1.064 | 1.048 | 0.939 | 12.63 | 11.32 | 0.184 | 0.205 |
| 1s180 | 1.184 | 1.141 | 0.844 | 0.876 | 10.18 | 10.56 | 0.229 | 0.220 |
| 2s0 | 0.925 | 0.991 | 1.081 | 1.009 | 13.03 | 12.16 | 0.179 | 0.191 |
| 2s30 | 0.983 | 0.990 | 1.017 | 1.010 | 12.26 | 12.17 | 0.190 | 0.191 |
| 2s60 | 0.958 | 0.913 | 1.043 | 1.095 | 12.58 | 13.20 | 0.185 | 0.176 |
| 2s90 | 0.989 | 1.015 | 1.011 | 0.985 | 12.18 | 11.87 | 0.191 | 0.196 |
| 2s120 | 0.878 | 1.021 | 1.138 | 0.979 | 13.72 | 11.80 | 0.169 | 0.197 |
| 2s180 | 0.928 | 2.834 | 1.077 | 0.352 | 12.98 | 4.251 | 0.179 | 0.195 |
| 4s0 | 1.020 | 1.013 | 0.980 | 0.987 | 11.81 | 11.89 | 0.197 | 0.196 |
| 4s30 | 0.997 | 1.077 | 1.003 | 0.928 | 12.08 | 11.19 | 0.192 | 0.208 |
| 4s60 | 0.924 | 0.923 | 1.082 | 1.083 | 13.04 | 13.05 | 0.178 | 0.178 |
| 4s90 | 0.939 | 0.941 | 1.064 | 1.062 | 12.83 | 12.80 | 0.181 | 0.182 |
| 4s120 | 0.990 | 0.992 | 1.010 | 1.008 | 12.17 | 12.14 | 0.191 | 0.191 |
| 4s180 | 0.991 | 1 | 1.009 | 1 | 12.16 | 12.05 | 0.191 | 0.193 |

*s: Time taken to acquire 1000 PIV images, 83 s.

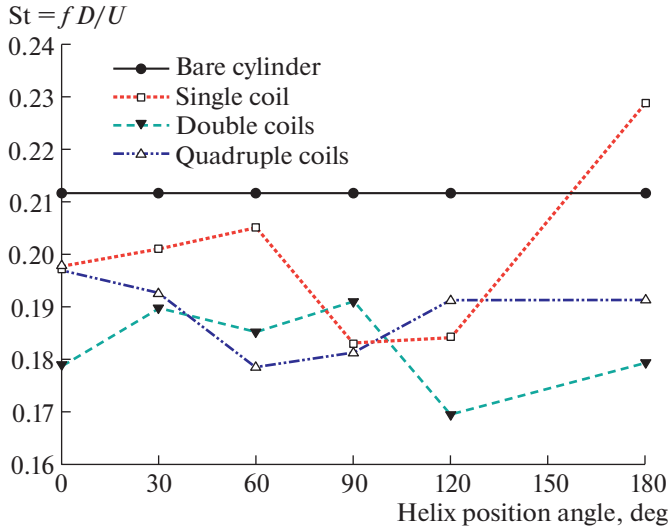


**Fig. 17.** Strouhal number versus the helix angle position.

decreasing the flow frequency and the corresponding St number. It is also concluded that the lower values of the St number increase the vibration absorption capability as a result of the lower natural frequency.

## ACKNOWLEDGMENTS

This study was supported by University Scientific Research Projects (CUBAP) commission within the scope of project M-728.

## REFERENCES

1. Prandtl, L., Über Flussigkeitsbewegung bei sehr kleiner Reibung, *Intern. Math. Kongr. Heidelberg*, 1904, pp. 484–491.
2. Chutkey, K., Suriyanarayanan, P., and Venkatakrishnan, L., Near wake field of circular cylinder with a forward splitter plate, *J. Wind Eng. Ind. Aerodyn.*, 2018, vol. 173, no. 2, pp. 28–38.
3. Liang, S., Wang, J., Xu, B., Wu, W., and Lin, K., Vortex-induced vibration and structure instability for a circular cylinder with flexible splitter plates, *J. Wind Eng. Ind. Aerodyn.*, 2018, vol. 174, no. 3, pp. 200–209.
4. Oruc, V., Akilli, H., and Sahin, B., PIV measurements on the passive control of flow past a circular cylinder, *Exp. Therm. Fluid Sci.*, 2016, vol. 70, pp. 283–291.
5. Durhasan, T., Aksoy, M.M., Pinar, E., Ozkan, G.M., Akilli, H., and Sahin, B., Vortex street suppression of a circular cylinder using perforated semi-circular fairing in shallow water, *Exp. Therm. Fluid Sci.*, 2016, vol. 79, pp. 101–110.
6. Ren, H., Xu, Y., Zhang, M., Fu, S., Meng, Y., and Huang, C., Distribution of drag coefficients along a flexible pipe with helical strakes in uniform flow, *Ocean Eng.*, 2019, vol. 184, pp. 216–226.
7. Zhang, H. and Shi, W., Numerical simulation of flow over a circular cylinder with a splitter plate near a moving wall, *Ocean Eng.*, 2016, vol. 122, pp. 162–171.
8. Xing, Y., Liu, P., Guo, H., and Li, L., Effect of helical cables on cylinder noise control, *Appl. Acoust.*, 2017, vol. 122, pp. 152–155.
9. Firat, E., Ozkan, G.M., and Akilli, H., PIV measurements in the near wakes of hollow cylinders with holes, *Exp. Fluids*, 2017, vol. 58, no. 5, pp. 1–19.
10. Li, L., Liu, P., Xing, Y., and Guo, H., Experimental investigation on the noise reduction method of helical cables for a circular cylinder and tandem cylinders, *Appl. Acoust.*, 2019, vol. 152, pp. 79–87.
11. Korkischko, I. and Meneghini, J.R., Experimental investigation of flow-induced vibration on isolated and tandem circular cylinders fitted with strakes, *J. Fluids Struct.*, 2010, vol. 26, no. 4, pp. 611–625.
12. Gozmen, B., Akilli, H., and Sahin, B., Passive control of circular cylinder wake in shallow flow, *Measurement*, 2013, vol. 46, no. 3, pp. 1125–1136.
13. Huang, S., VIV suppression of a two-degree-of-freedom circular cylinder and drag reduction of a fixed circular cylinder by the use of helical grooves, *J. Fluids Struct.*, 2011, vol. 27, no. 7, pp. 1124–1133.

14. Ekmekci, A., Circular cylinders fitted with small-scale straight and helical wires: A comparative study on the wire-induced critical effects, *Exp. Therm. Fluid Sci.*, 2014, vol. 53, pp. 179–189.
15. Liu, K., Deng, J., and Mei, M., Experimental study on the confined flow over a circular cylinder with a splitter plate, *Flow Meas. Instrum.*, 2016, vol. 51, pp. 95–104.
16. Particle Image Velocimetry (PIV) Measurement Systems, [Online]. Available: https://www.dantecdynamics.com/particle-image-velocimetry [Accessed: 26-Jun-2020].
17. Akilli, H., Sahin, B., and Tumen, N.F., Suppression of vortex shedding of circular cylinder in shallow water by a splitter plate, *Flow Meas. Instrum.*, 2005, vol. 16, no. 4, pp. 211–219.
18. Dong, S., Karniadakis, G.E., Ekmekci, A., and Rockwell, D., A combined direct numerical simulation–particle image velocimetry study of the turbulent near wake, *J. Fluid Mech.*, 2006, vol. 569, pp. 185–207.
19. Canpolat, C. and Sahin, B., Influence of single rectangular groove on the flow past a circular cylinder, *Int. J. Heat Fluid Flow*, 2017, vol. 64, pp. 79–88.
20. Yagmur, S., Dogan, S., Aksoy, M.H., Goktepeli, I., and Ozgoren, M., Comparison of flow characteristics around an equilateral triangular cylinder via PIV and Large Eddy Simulation methods, *Flow Meas. Instrum.*, 2017, vol. 55, pp. 23–36.
21. Ozgoren, M., Okbaz, A., Dogan, S., Sahin, B. and Akilli, H., Investigation of flow characteristics around a sphere placed in a boundary layer over a flat plate, *Exp. Therm. Fluid Sci.*, 2013, vol. 44, no. 8, pp. 62–74.
22. Blevins, R.D., *Flow-induced vibration*, 2nd ed., New York: Van Nostrand Reinhold, 1990.